ACS APPLIED MATERIALS & INTERFACES

Research Article

www.acsami.org

Template-Free Fabrication of TiO_2 Hollow Spheres and Their Photocatalytic Properties

Shuqin Shang, Xiuling Jiao, and Dairong Chen*

Key Laboratory for Special Functional Aggregate Materials of Education Ministry, School of Chemistry and Chemical Engineering, Shandong University, Jinan 250100, P. R. China

Supporting Information

ABSTRACT: Submicrometer-sized anatase TiO_2 hollow spheres were fabricated through a template-free solvothermal route using $TiCl_4$ as a raw material and a mixture of alcohols–acetone as solvent. Control of the hollow spheres' size was achieved by adjusting the ratio of alcohols to acetone. Products were characterized by scanning electron microscopy (SEM), transmission electron microscopy (TEM), high resolution TEM, X-ray photoelectron spectra (XPS), X-ray diffraction (XRD), Fourier transform infrared (FT-IR), and thermogravimetric (TG) analysis. It was found that the formation process of the TiO_2 hollow spheres might include the hydrolysis of Ti(IV) with the water formed from the solvothermal etherification reaction, the aggregation of the anatase TiO_2 nanoparticles, and the Ostwald ripening. Furthermore, the as-prepared TiO_2 hollow nanostructures exhibited good photocatalytic activity for the degradation of phenol.

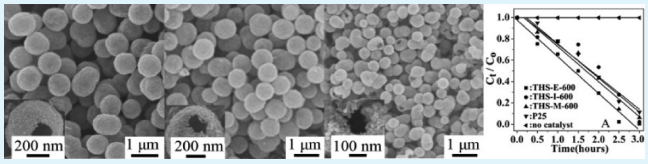

KEYWORDS: *TiO_2, hollow spheres, nanostructures, template-free fabrication, photocatalysis*

INTRODUCTION

As an n-type semiconductor, TiO_2 (titania) has extensive applications in photocatalysis and conversion of solar energy because of its high refractive index, wide band gap, chemical stability, and low cost.[1−4] Since the 1970s when Fujishima and Honda first reported that water could be decomposed to H_2 and O_2 on the TiO_2/Pt electrode in a photoelectrochemical system, the photocatalytic property of TiO_2 has aroused great interest.[5] TiO_2 can effectively photodegrade many pollutants in air or water because of its wide band gap and high photocatalytic activity.[6−8] To improve the photocatalytic property, many anatase TiO_2 nanostructures with high surface area or mesoporous structure have been fabricated,[9−12] of which hollow spheres have attracted much attention in the fields of catalysis, microreactors, adsorption, and drug delivery.[13]

To date, a variety of hard templates such as silica,[14−19] polymer spheres,[20−39] carbon,[40−45] and $CaCO_3$ spheres[46,47] or soft templates such as microemulsion droplets,[48] ionic liquids,[49] and bubbles[50−53] have been applied to direct the formation of hollow spheres by adsorption or chemical reaction on their surfaces, which have proven to be effective routes to many hollow nanostructures. These methods generally require multistep processes, in which the template will be removed by calcination or dissolution. Therefore, the template-free method for the control synthesis of hollow nanostructures shows some advantages because of a simple and relatively environment-friendly process.[54−61] Recently, several strategies for synthesizing TiO_2 hollow nanostructures by a template-free route have been attempted. Li et al. solvothermally synthesized hollow TiO_2 spheres with unique urchin-like morphology and tunable interior structure in glycerol, alcohol, and ethyl ether using $TiOSO_4$ as a raw material.[54] Zeng et al. prepared anatase TiO_2 hollow microspheres by the hydrothermal reaction of TiF_4 in the presence of additives such as thioueа, urea, and HF.[55] Mann et al. prepared well-defined TiO_2 hollow spheroids through a hydrothermal method using $TiOSO_4$ as a precursor and NH_4F as an additive, in which the self-transformation of amorphous TiO_2 microparticles to hollow architecture was promoted by fluoride-mediated surface dissolution and recrystallization of the amorphous primary particles.[60] More recently, hollow TiO_2 spheres with selective photocatalytic property were fabricated using a fluoride mediated self-transformation method and designed surface chemistry, which is a significant improvement in researching the photocatalytic performance of titania.[61] Although progress in the template-free fabrication of hollow TiO_2 nanostructures has been achieved, the control in size and performance still remains a great challenge. Therefore, the development of an efficient template-free route is desirable for the fabrication of hollow TiO_2 nanostructures.

EXPERIMENTAL SECTION

Synthesis. Absolute ethanol was dehydrated by Mg powder and I_2 before being used, and isopropanol, methanol, and acetone were dehydrated by anhydrous calcium sulfate. In a typical synthesis, 10.0 mL of absolute ethanol and 2.5 mL of acetone were sequentially added into 0.1 mL of $TiCl_4$ with stirring to form a colorless transparent solution in a flask. The solution was transferred to a 20 mL autoclave with a Teflon linear and heated at 220 °C for 12 h. Then, it was cooled to room temperature, and the product was separated by centrifugation

Received: November 3, 2011
Accepted: December 29, 2011
Published: December 29, 2011

and twice washed with anhydrous ethanol and deionized water. Finally, the sample was dried at 60 °C in air for 6 h. The resulting sample was labeled as THS-E. To remove the adsorbed organics, the sample was heated at 600 °C for 1.5 h with a heating rate of 2.0 °C/min from 30 to 600 °C before being used as a photocatalyst, which was denoted as THS-E-600.

Characterization. The morphology and microstructure of the products were characterized using a transmission electron microscope (TEM, JEM 100-CXII) with an accelerating voltage of 80 kV, a field-emission scanning electron microscope (FE-SEM, JSM-6700F), and a high resolution TEM (HR-TEM, GEOL-2010) with an accelerating voltage of 200 kV. X-ray diffraction (XRD) patterns were collected on a Rigaku D/Max 2200PC diffractometer with a graphite monochromator and CuKα radiation (λ = 0.15418 nm). A microtome (Reichert/Jung Ultracut E, Leica, Arcadia, CA) equipped with a diamond knife was used to cut the cured epoxy resin into slices with a thickness of 80 nm. The slices were placed on copper grids for HR-TEM observations. Thermogravimetric (TG) analysis was carried out at a heating rate of 10 °C/min from room temperature to 1200 °C under an air atmosphere (Mettler Toledo, TGA/SDTA 851e). Fourier-transform infrared (FT-IR) spectra were recorded on a Nicolet 5DX FT-IR spectrometer using KBr pellet technique in the range of 4000−400 cm^{-1}. N_2 adsorption−desorption isotherms were measured on a QuadraSorb (Supporting Information) apparatus at 77 K, and before measurement, the samples were degassed in a vacuum at 100 °C for 12 h. The surface area was calculated using the Brunauer−Emmett−Teller (BET) method, and pore size distribution was calculated from the desorption branch using the Barrett−Joyner−Halenda (BJH) theory. Gas chromatograph mass spectrometer (GC-MS) analysis was performed on Shimadzu GC-MS-QP 2010. X-ray photoelectron spectroscopy (XPS) spectra were recorded on a PHI-5300 ESCA spectrometer (Perkin-Elmer) with its energy analyzer working in the pass energy mode at 35.75 eV, and the AlK line was used as the excitation source. The binding energy reference was taken at 284.7 eV for the C1s peak arising from surface hydrocarbons.

Photocatalytic Activity. Photocatalytic performance of the calcined product was characterized by the photodegradation of phenol in water. Into 40.0 mL of phenol solution (65.2 mg/L) in a 50 mL quartz reaction container, 40.0 mg of the sample was added and stirred for 2 h under shade conditions. Then, the solution was irradiated using a high-pressure mercury lamp (200 W, λ_{max} = 365 nm, λ = 320−400 nm) for a period of time. A UV−vis absorption spectrometer (Lambda-35, Perkin-Elmer) was applied to detect the concentration of phenol according to the change of the absorption intensity at 270 nm.

RESULTS AND DISCUSSION

Structure and Morphology of the TiO_2 Hollow Spheres. TEM and FE-SEM images (Figure 1a,b) indicate the presence of uniform hollow structures with a wall thickness of 40−60 nm and a diameter of 0.8−1.0 μm. FE-SEM and HR-TEM images (Figure 1a inset, Figure 1c and its inset) show that the hollow spheres are randomly aggregated by the TiO_2 nanoparticles of ca. 20 nm. The nanoparticles are octahedral double cones with some 3−4 nm particles attached on the surfaces. The interplanar distance of 0.236 nm corresponds to the (004) plane of anatase TiO_2. For natural anatase mineral crystals, these little bipyramidal crystals also exhibited low-energy growth surfaces with (101) facets.[62] The XRD pattern of the solvothermal product (Figure1d) shows that all the reflections could be indexed to tetragonal anatase TiO_2 (JCPDS No.21-1272), and no peaks of impurities were observed, indicating the anatase phase-pure nature of the product.

The IR spectrum (Figure 2a) of the solvothermal hollow TiO_2 spheres shows absorptions at 2859, 2927, 1262, and 1000−1200 cm^{-1} together with the strongest absorption of the Ti−O bond at 456 cm^{-1}. These absorptions can be attributed to the vibrations of C−H, C−O, and C−O−C bonds,

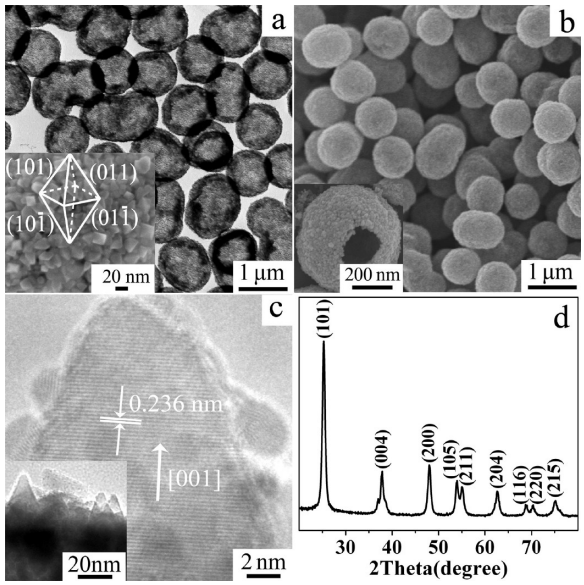

Figure 1. TEM (a), SEM (b), and HR-TEM (c) images and (d) XRD pattern of the solvothermal product (THS-E). The insets in a, b, and c are, respectively, the images of a sphere's surface, a broken hollow sphere, and the local surface of a hollow sphere.

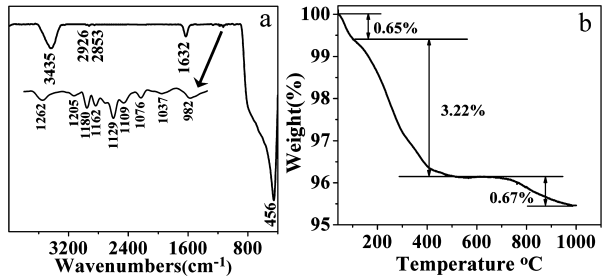

Figure 2. IR spectrum (a) and TG curve (b) of the TiO_2 hollow spheres THS-E.

indicating the existence of organic molecules on the spheres' surface. The band around 3435 cm^{-1} is associated with the asymmetric and symmetric stretching vibrations of the −OH group of absorbed water molecules and the surface hydroxyls of the TiO_2 particles, and that at 1632 cm^{-1} is assigned to the bending vibrations of the water molecules.[63] The TG curve (Figure 2b) shows the weight loss of the product. From room temperature to 110 °C, the weight loss of 0.65% is due to the elimination of the physically adsorbed water. The weight loss of 3.22% from 110 to 450 °C is attributed to the decomposition of the organics[64] and chemisorbed water molecules desorption.[65] That appearing at 700−980 °C with an amount of 0.67% can be ascribed to the removal of the surface hydroxyls.[66] The IR and TG results reveal that there are small amounts of absorbed water, organics, and hydroxyls on the hollow spheres' surface.

Formation of TiO_2 Hollow Spheres. The formation process of hollow spheres was tracked to investigate the formation mechanism (Figure 3). It was found that the solid spheres with a smooth surface were formed after the solvothermal reaction was conducted for 1 h. The XRD pattern demonstrates that the product is poor-crystalline anatase TiO_2 (Figure 3h). The corresponding typical type I adsorption isotherm indicates that the sample has many micropores with a size of 1.39 nm (Figure S1a, Supporting Information)[67] and a BET surface area of 262 m^2/g. When the

dx.doi.org/10.1021/am201535u | ACS Appl. Mater. Interfaces 2012, 4, 860−865

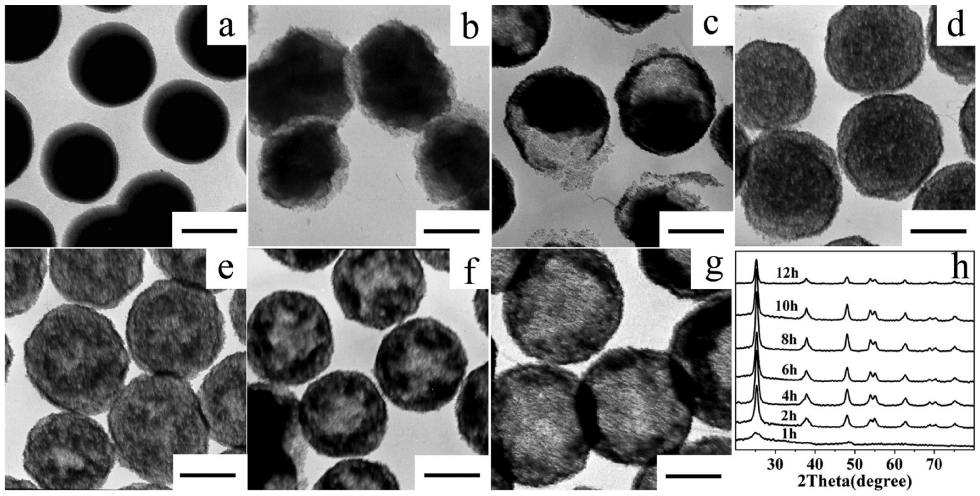

Figure 3. TEM images of the solvothermal samples after a solvothermally reaction at 220 °C for 1 h (a), 2 h (b), 4 h (c), 6 h (d), 8 h (e), 10 h (f), and 12 h (g), and the corresponding XRD patterns (h), (all scale bars = 500 nm).

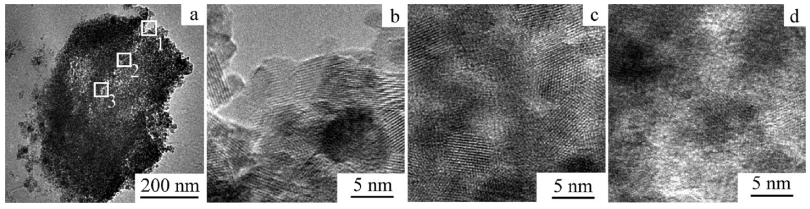

Figure 4. TEM (a) and HR-TEM (b, c, d) images of the sliced solvothermal product obtained at 220 °C for 2 h (b, c, and d, respectively, correspond to the region indicated by squares 1, 2, and 3 in a).

reaction was conducted for 2 h, the spheres' surface became very coarse, and the crystallinity of the anatase TiO_2 significantly increased from the XRD pattern (Figure 3h), while at the same time the BET surface area of the product was reduced to 181 m^2/g (Figure S1b, Supporting Information). When the solvothermal reaction time increased to 4 h, partly empty spheres were produced. Further prolonging the reaction time, the interior of the spheres gradually became empty and the shell gradually formed. Finally, the hollow spheres were formed when the solvothermal reaction was conducted for 12 h (Figure 3g), while the surface area of spheres decreased to 114 m^2/g. IR spectra reveal that some organics in the solid spheres are gradually reduced with the length of reaction time and the transformation from solid spheres to hollow ones (Figure S2, Supporting Information). In addition, the 1 h solvothermal product was separated and then solvothermally treated for 12 h in the same solvent as the main experiment, and hollow spheres were also obtained.

From the above experiments, it is proposed that the formation of the TiO_2 hollow spheres goes through the formation of poorly crystallized solid spheres and the transformation of the solid spheres to hollow ones is based on the Ostwald ripening process. During the transformation to the hollow spheres, the inner part of the solid spheres gradually dissolved and was recrystallized on the shell of the spheres to finally form hollow spheres. To further clarify the driving force of this Ostwald ripening, the solid spheres obtained at 2 h were observed by the HR-TEM technique after being cut by a diamond knife (Figure 4). It was observed that the solid sphere was composed of irregularly arranged TiO_2 nanoparticles with a size of 5−10 nm. Further observation of different areas of a single sphere indicated that the crystallinity of the nanoparticles gradually increased from the interior to the exterior of the shell. This crystallinity difference might be due to the surrounding polar solvent, which favored the crystallization of the TiO_2. Because the less-crystalline particles inside the solid spheres are more likely to dissolve, the dissolution of the interior of the solid spheres and recrystallization on the surface of the spheres occurred, and finally, the hollow structures were formed.

It is reported that the Ostwald ripening process usually occurs in the presence of water. In the present experiment, no water was added, so the GC-MS analysis of the supernatant solution was conducted after being solvothermally treated for 12 h. As evinced by the GC-MS analysis, ethyl ether exists in the supernatant solution after being solvothermally treated for 12 h, indicating that part of the ethanol was transformed to ether, and water was also generated at the same time (eq 1). Therefore, it can be inferred that the Ostwald ripening process was promoted by the self-generated water during the solvothermal process.

$$2CH_3CH_2OH \xrightarrow[200-220^\circ C]{TiCl_4} CH_3CH_2OCH_2CH_3 + H_2O \quad (1)$$

Further experimentation revealed that adding water into the solvothermal system can accelerate the formation of hollow spheres. For example, when 7−9 μL of water was added, hollow spheres would form only after reacting for 6 h (Figure 5a,b). However, more water (11−18 μL) resulted in the formation of the partly empty TiO_2 structures (Figure 5c,d). The core cannot disappear even if the solvothermal reaction time was extended to 12 days, which might be due to the relative higher crystallinity of the inner particles formed in the presence of more water.

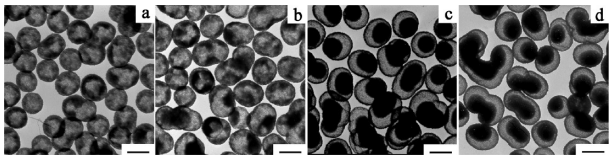

Figure 5. TEM images of the products by the ethanol–acetone system reacting at 220 °C with different water contents: (a) 7 μL, (b) 9 μL, (c) 11 μL, and (d) 14 μL (all scale bars = 1 μm).

On the basis of the above analyses, the formation mechanism of the TiO_2 hollow spheres is schematically presented in Figure 6. Under solvothermal conditions, the reaction shown in eq 1 occurred, and the formed water promoted the hydrolysis of Ti(IV) to form anatase TiO_2 nanoparticles with poor crystallinity because of the small water content. These particles quickly aggregated to form solid spheres because of the high surface energy. Due to the continuous formation of water and the water content gradually increasing in the system, the surface nanoparticles exhibited relative higher crystallinity, which was at the shell of the spheres. Then, with the release of water, the dissolution of the less-crystallized inner particles and the recrystallization on the spheres' shell was carried out. Finally, TiO_2 hollow spheres with high crystallinity were formed.

Fabrication of TiO_2 Hollow Spheres with Different Sizes. It can be seen that water plays a critical role in the formation of the hollow spheres, which mainly comes from the etherification of ethanol in the typical system. Different alcohols exhibit different etherification reaction rates in the system, which affect the formation and aggregation of primary TiO_2 nanocrystals, as well as the Ostwald ripening process of the solid spheres. Therefore, alcohols were adjusted in the present experiment in order to adjust the product size and microstructure. When one-fourth volume of ethanol was replaced by isopropanol, that is, the system contained 7.5 mL of ethanol, 2.5 mL of isopropanol, 2.5 mL of acetone, and 0.1 mL of $TiCl_4$, the hollow spheres decreased to 700–800 nm with a wall thickness of ca. 60 nm (Figure 7a,c), which was labeled as THS-I. The XRD pattern indicated that the product was also anatase TiO_2. HR-TEM images show that the primary nanoparticle was a truncated octahedron with an edge size of ca. 20 nm. When one-fourth volume of ethanol was replaced by methanol containing 12.0 μL of HF acid (38.0 wt %;the system contained 7.5 mL of ethanol, 2.5 mL of methanol, 2.5 mL of acetone, 12.0 μL of HF acid, and 0.1 mL of $TiCl_4$), hollow spheres with a diameter of 400–500 nm and a wall thickness of ca. 40 nm were formed (labeled as THS-M), which were aggregated by the irregular nanoparticles with broad size distribution besides the octahedrons (Figure 7b,d). Therefore, TiO_2 hollow spheres with sizes from 400 nm to 1 μm can be obtained by simply adjusting the alcohol in the solvothermal system.

Photocatalytic Activity. Photocatalytic activity of the calcined hollow spheres was evaluated using the photodegradation of toxic phenol. P25, a commercially available photocatalyst, was used as the reference. The UV–vis absorption at 270 nm was applied to determine the phenol concentration in the solution. The experimental results showed that the phenol concentration hardly changed without a catalyst under UV irradiation for 3 h. Using P25 as a catalyst, 84.5% of phenol was degraded after the phenol solution was irradiated by UV light for 3 h, and THS-I-600 and THS-M-600 exhibited similar catalytic activity with P25, while 99.9% was decomposed using THS-E-600 as the catalyst (Figure 8A). Moreover,

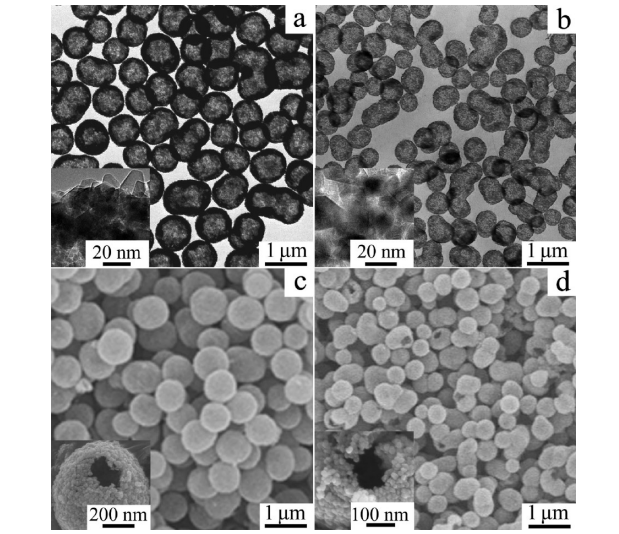

Figure 7. TEM and FE-SEM images of the products THS-I (a, c) and THS-M (b, d). (Insets are the corresponding HR-TEM and high-magnification SEM images.)

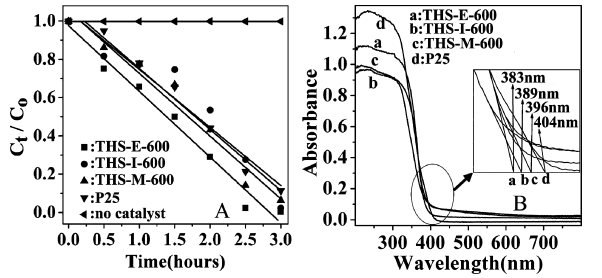

Figure 8. Phenol concentration changes as a function of UV irradiation time using different catalysts (A) and UV–vis absorption spectra of the calcined TiO_2 hollow spheres and P25 (B).

THS-E-600 not only possesses good photocatalytic activity but also can be reused several times without obvious change in catalytic activity.

As is known, many parameters such as primary particle size, surface area, crystal morphology, the exposed facet, surface state, and defects influence the photocatalytic properties of TiO_2 materials.[68–70] Thus, the surface area, pore volume, pore size, and average particle size of the products and P25 (15–30% rutile, 70–85% anatase) were determined and are listed in Table 1, which demonstrates that the products

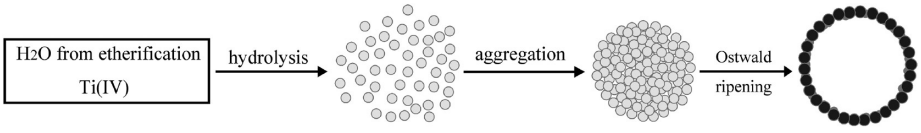

Figure 6. Schematical representation of the formation mechanism of TiO_2 hollow spheres.

dx.doi.org/10.1021/am201535u | ACS Appl. Mater. Interfaces 2012, 4, 860–865

Table 1. Properties of Products[a]

titania	surface area (m^2/g)	pore volume (cm^3/g)	pore size (nm)	average crystallite size (nm)
THS-E-600	58	0.26	7.0	17.2
THS-I-600	53	0.20	6.3	17.6
THS-M-600	52	0.19	8.3	17.7
P25	55			21.7

[a]Surface area, pore volume, pore diameter, and average particle size of the products. Surface area: BET surface area. Pore volume: BJH pore volume. Pore diameter: BJH pore diameter from nitrogen desorption branch. Average crystallite size: analysis of the peak broadening of the (101) reflection using the Scherrer equation.

THS-E-600, THS-I-600, and THS-M-600 exhibit similar surface area and pore volume to that of the P25. The UV–vis absorption spectra (Figure 8B) show that the absorption edges of the hollow spheres display obvious blue shifts relative to P25 powder, which might be due to the pure anatase composition or effect of the nanosize of the hollow spheres. The higher photocatalytic activity of TiO_2 hollow spheres may relate to the blue shift of the absorption edge. Ti2p and O1s binding energies were also determined to investigate the catalytic property of the hollow spheres. The XPS spectra (Figure 9) show

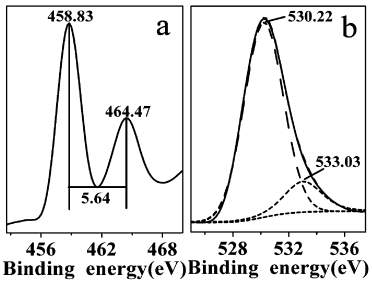

Figure 9. $Ti2p_{3/2}$ and $Ti2p_{1/2}$ (a) and O1s (b) peaks of XPS patterns of THS-E-600.

the $Ti2p_{3/2}$ level at 458.83 eV, and the spin–orbital splitting between $Ti2p_{3/2}$ and $Ti2p_{1/2}$ is 5.64 eV, which is in agreement with the reported value.[71,72] The O1s photoelectron peak may be resolved into two components: the major peak at 530.01 eV corresponds to the lattice oxygen, and that at 533.03 eV is mainly attributed to chemisorbed water or surface hydroxyls.[63] As is known, surface adsorbed water or surface hydroxyls play an important role in determining photocatalytic activity. In photocatalysis reactions, surface adsorbed water or the hydroxyl group can capture the photogenerated hole, forming oxidative hydroxyl radicals, prevent electron–hole recombination, and therefore increase photocatalytic activity.[73]

CONCLUSIONS

In summary, well-dispersed submicrometer-sized TiO_2 hollow spheres with different sizes were synthesized using a simple template-free method. The formation process of the hollow spheres went through the hydrolysis of the poor-crystallized TiO_2 nanoparticles and their aggregation to solid spheres, as well as the following dissolution–recrystallization processes. Control of the size of the hollow spheres can be achieved by simply adjusting the percentage of alcohol in the system. The hollow nanostructures showed superior photocatalytic activity on the degradation of phenol compared to Degussa P25.

ASSOCIATED CONTENT

Supporting Information

N_2 adsorption–desorption isotherms and pore size distributions of products by the $TiCl_4$–ethanol–acetone system; IR spectra of the solvothermal products by the ethanol–acetone system. This material is available free of charge via the Internet at http://pubs.acs.org.

AUTHOR INFORMATION

Corresponding Author

*E-mail: cdr@sdu.edu.cn. Fax:+86-0531-88364281. Tel: +86-0531-88364280.

ACKNOWLEDGMENTS

This work is supported by the Major State Basic Research Development Program of China (973 Program) (No.2010CB933504), the Science Funds for Distinguished Young Scientists of Shandong Province (JQ200903), and the Natural Science Foundation of Shandong Province (No. ZR2011BZ002). We thank Dr. Edward C. Mignot for help in revising the whole text for English.

REFERENCES

(1) Fujishima, A.; Rao, T.; Tryk, D. A. *J. Photochem. Photobiol., C* **2000**, *1*, 1.
(2) Diebold, U. *Surf. Sci. Rep.* **2003**, *48*, 53.
(3) Thompson, T. L.; Yates, J. T. *Chem. Rev.* **2006**, *106*, 4428.
(4) Chen, X.; Mao, S. *Chem. Rev.* **2007**, *107*, 2891.
(5) Fujishima, A.; Honda, K. *Nature* **1972**, *238*, 37.
(6) Pillai, S. C.; Periyat, P.; George, R.; Mccormack, D. E.; Seery, M. K.; Hayden, H.; Colreavy, J.; Corr, D.; Hinder, S. J. *J. Phys. Chem. C* **2007**, *111*, 1605.
(7) Periyat, P.; Baiju, K. V.; Mukundan, P.; Pillai, P. K.; Warrier, K. G. K. *Appl. Catal., A: Gen.* **2008**, *349*, 13.
(8) Sakatani, Y.; Grosso, D.; Nicole, L.; Boissière, C.; Soler-Illia, Galo J. de A. A.; Sanchez, C. *J. Mater. Chem.* **2006**, *16*, 77.
(9) Zhao, Z.; Jiao, X.; Chen, D. *J. Mater. Chem.* **2009**, *19*, 3078.
(10) Sun, J.; Gao, L.; Zhang, Q. *J. Am. Ceram. Soc.* **2003**, *86*, 1677.
(11) Cheewita, S.; Sumpun, W. *J. Nanopart. Res.* **2010**, *12*, 2895.
(12) Chi, B.; Zhao, L.; Jin, T. *J. Phys. Chem. C* **2007**, *111*, 6189.
(13) Lou, X.; Archer, L. A.; Yang, Z. *Adv. Mater.* **2008**, *20*, 3987.
(14) Kai, Z.; Zhang, X.; Chen, H.; Chen, X.; Zheng, L.; Zhang, J.; Yang, B. *Langmuir* **2004**, *20*, 11312.
(15) Zhu, Y.; Cao, Y.; Li, Z.; Ding, J.; Liu, J.; Chi, Y. *J. Colloid Interface Sci.* **2007**, *306*, 133.
(16) Kim, H.; Choi, K.; Shul, Y. *Korean J. Chem. Eng.* **2007**, *24*, 596.
(17) Yu, J.; Liu, W.; Yu, H. *Crystal Growth Des.* **2008**, *8*, 930.
(18) Nelson, K.; Deng, Y. *Langmuir* **2008**, *24*, 975.
(19) Wang, D.; Zeng, H. *Chem. Mater.* **2009**, *21*, 4811.
(20) Zhong, Z.; Yin, Y.; Gates, B.; Xia, Y. *Adv. Mater.* **2000**, *12*, 206.
(21) Caruso, R. A.; Susha, A.; Caruso, F. *Chem. Mater.* **2001**, *13*, 400.
(22) Yin, Y.; Lu, Y.; Gates, B.; Xia, Y. *Chem. Mater.* **2001**, *13*, 1146.
(23) Imhof, A. *Langmuir* **2001**, *17*, 3579.
(24) Caruso, F.; Shi, X.; Caruso, R. A.; Susha, A. *Adv. Mater.* **2001**, *13*, 740.
(25) Wang, L.; Sasaki, T.; Ebina, Y.; Kurashima, K.; Watanabe, M. *Chem. Mater.* **2002**, *14*, 4827.
(26) Yang, Z.; Niu, Z.; Lu, Y.; Hu, Z.; Han, C. C. *Angew. Chem., Int. Ed.* **2003**, *42*, 1943.
(27) Li, Y.; Kunitake, T.; Fujikawa, S. *J. Phys. Chem. B* **2006**, *110*, 13000.
(28) Cheng, X.; Chen, M.; Wu, L.; Gu, Y. *Langmuir* **2006**, *22*, 3858.
(29) Song, X.; Gao, L. *J. Phys. Chem. C* **2007**, *111*, 8180.
(30) Song, X.; Gao, L. *Langmuir* **2007**, *23*, 11850.
(31) Li, H.; Ha, C.; Kim, I. *Langmuir* **2008**, *24*, 10552.

(32) Kartsonakis, I. A.; Liatsi, P.; Danilidis, I.; Bouzarelou, D.; Kordas, G. *J. Phys. Chem. Solids* **2008**, *69*, 214.
(33) Chung, C.; Jean, J. H. *J. Am. Ceram. Soc.* **2008**, *91*, 3074.
(34) Yang, J.; Lind, J.; Trogler, W. *Chem. Mater.* **2008**, *20*, 2875.
(35) Peng, B.; Meng, X.; Tang, F.; Ren, X.; Chen, D.; Ren, J. *J. Phys. Chem. C* **2009**, *113*, 20240.
(36) Agrawal, M.; Gupta, S.; Pich, A.; Zafeiropoulost, N. E.; Stam, M. *Chem. Mater.* **2009**, *21*, 5343.
(37) Li, X.; Lv, K.; Deng, K.; Tang, J.; Su, R.; Sun, J.; Chen, L. *Mater. Sci. Eng., B* **2009**, *158*, 40.
(38) Yao, L.; Shi, Y.; Jin, S.; Li, M.; Zhang, L. *Mater. Res. Bull.* **2010**, *45*, 1351.
(39) Zhang, D.; Yang, D.; Zhang, H.; Lu, C.; Qi, L. *Chem. Mater.* **2006**, *18*, 3477.
(40) Ao, Y.; Xu, J.; Fu, D.; Yuan, C. *Catal. Commun.* **2008**, *9*, 2574.
(41) Ao, Y.; Xu, J.; Fu, D.; Yuan, C. *J. Hazard. Mater.* **2009**, *167*, 413.
(42) Ao, Y.; Xu, J.; Fu, D.; Yuan, C. *Microporous Mesoporous Mater.* **2009**, *118*, 382.
(43) Xu, J.; Ao, Y.; Chen, M. *Mater. Lett.* **2009**, *63*, 2442.
(44) Wang, J.; Bai, Y.; Wu, M.; Yin, J.; Zhang, W. *J. Power Sources* **2009**, *191*, 614.
(45) Wang, H.; Wu, Z.; Liu, Y. *J. Phys. Chem. C* **2009**, *113*, 13317.
(46) Gao, L.; Luo, L.; Chen, J.; Shao, L. *Chem. Lett.* **2005**, *34*, 138.
(47) Bala, H.; Yu, Y.; Zhang, Y. *Mater. Lett.* **2008**, *62*, 2070.
(48) Collins, A. M.; Spickermann, C.; Mann, S. *J. Mater. Chem.* **2003**, *13*, 1112.
(49) Nakashima, T.; Kimizuka, N. *J. Am. Chem. Soc.* **2003**, *125*, 6386.
(50) Li, X.; Xiong, Y.; Li, Z.; Xie, Y. *Inorg. Chem.* **2006**, *45*, 3493.
(51) Kim, Y.; Chai, S.; Lee, W. *Langmuir* **2007**, *23*, 9567.
(52) Liu, L.; Cui, Y.; Li, B.; Zhou, X.; Ding, W. *Appl. Surf. Sci.* **2010**, *256*, 2596.
(53) Feng, X.; Yang, L.; Liu, Y. *Mater. Lett.* **2010**, *64*, 2688.
(54) Li, H.; Bian, Z.; Zhu, J.; Zhang, D.; Li, G.; Huo, Y.; Li, H.; Lu, Y. *J. Am. Chem. Soc.* **2007**, *129*, 8406.
(55) Yang, H.; Zeng, H. *J. Phys. Chem. B* **2004**, *108*, 3492.
(56) Yang, H.; Zeng, H. *Angew. Chem., Int. Ed.* **2004**, *43*, 5206.
(57) Wang, X.; Xiao, P. *J. Mater. Res.* **2005**, *20*, 796.
(58) Pan, J.; Zhang, X.; Du, J.; Sun, D.; Leckie, J. O. *J. Am. Chem. Soc.* **2008**, *130*, 11256.
(59) Yu, J.; Zhang, J. *Dalton Trans.* **2010**, *39*, 5860.
(60) Yu, J.; Guo, H.; Davis, S. A.; Mann, S. *Adv. Eng. Mater.* **2006**, *16*, 2035.
(61) Liu, S.; Yu, J.; Jaroniec, M. *J. Am. Chem. Soc.* **2010**, *132*, 11914.
(62) Lu, Y.; Jaeckel, B.; Parkinson, B. A. *Langmuir* **2006**, *22*, 4472.
(63) Liu, S.; Sun, X.; Li, J.; Li, X.; Xiu, Z.; Yang, H. *Langmuir* **2010**, *26*, 4546.
(64) Jiang, X.; Herricks, T.; Xia, Y. *Adv. Mater.* **2003**, *15*, 1205.
(65) Yaghoubi, H.; Taghavinia, N.; Alamdari, E. K.; Volinsky, A. A. *ACS Appl. Mater. Interfaces* **2010**, *2*, 2629.
(66) Liu, J.; Hu, Y.; Gu, F.; Li, C. *Ind. Eng. Chem. Res.* **2009**, *48*, 735.
(67) Sing, K. S. W.; Everett, D. H. R.; Haul, A. W.; Mosou, L.; Pierotti, R. A.; Rouquerol, J.; Siemieniewska, T. *Pure Appl. Chem.* **1985**, *57*, 603.
(68) Carp, O.; Huisman, C. L.; Reller, A. *Prog. Solid State Chem.* **2004**, *32*, 33.
(69) Yang, H.; Sun, C.; Qiao, S.; Zou, J.; Liu, G.; Smith, S. C.; Cheng, H.; Lu, G. *Nature* **2008**, *453*, 638.
(70) Han, X.; Kuang, Q.; Jin, M.; Xie, Z.; Zheng, L. *J. Am. Chem. Soc.* **2009**, *131*, 4078.
(71) Moulder, J. F.; Stickle, W. F.; Sobol, P. E.; Bomben, K. D. *Handbook of X-ray Photoelectron Spectroscopy*; Perkin-Elmer Corp.: Eden Prairie, MN, 1992.
(72) Nagaveni, K.; Hegde, M. S.; Ravishanker, N.; Subbanna, G. N.; Madras, G. *Langmuir* **2004**, *20*, 2900.
(73) Yu, J.; Wang, X.; Fu, X. *Chem. Mater.* **2004**, *16*, 1523.